Stochastic modeling of neurobiological time series: Power, coherence, Granger causality, and separation of evoked responses from ongoing activity

Yonghong Chen
The J. Crayton Pruitt Family Department of Biomedical Engineering, University of Florida, Gainesville, Florida 32611

Steven L. Bressler
Center for Complex Systems and Brain Sciences, Florida Atlantic University, Boca Raton, Florida 33431

Kevin H. Knuth
Department of Physics, State University of New York at Albany, Albany, New York 12222

Wilson A. Truccolo
Neuroscience Department, Brown University, Providence, Rhode Island 02912

Mingzhou Ding
The J. Crayton Pruitt Family Department of Biomedical Engineering, University of Florida, Gainesville, Florida 32611

(Received 6 March 2006; accepted 7 May 2006; published online 30 June 2006)

In this article we consider the stochastic modeling of neurobiological time series from cognitive experiments. Our starting point is the variable-signal-plus-ongoing-activity model. From this model a differentially variable component analysis strategy is developed from a Bayesian perspective to estimate event-related signals on a single trial basis. After subtracting out the event-related signal from recorded single trial time series, the residual ongoing activity is treated as a piecewise stationary stochastic process and analyzed by an adaptive multivariate autoregressive modeling strategy which yields power, coherence, and Granger causality spectra. Results from applying these methods to local field potential recordings from monkeys performing cognitive tasks are presented. © *2006 American Institute of Physics*. [DOI: 10.1063/1.2208455]

In a typical cognitive experiment, the subject often performs the same task repeatedly and each repetition is called a trial. The recorded neurophysiological signals exhibit large variability from trial to trial. Traditionally, it has been assumed that (1) the evoked response is invariant across trials and (2) the trial-to-trial variability is due to background noise. The analysis method has thus been to average the single-trial time series across an ensemble of trials, triggered either on the stimulus onset or the movement onset, to attenuate the effect of noise and enhance the evoked signal. This event-related potential (ERP) strategy has been the dominant approach in cognitive neuroscience. Evidence over the past few years has begun to challenge the two assumptions underlying this strategy. In this article we review recent results in this area starting with the introduction of a generative signal model of event-related recordings. We proceed to discuss statistical strategies for estimating the parameters in the model. Examples of applying the analysis framework to local field potential data recorded from monkeys performing a visuomotor task are included. With suitable generalization, data from genetic networks may also be analyzed within the framework discussed here.

I. INTRODUCTION

Cognitive functions are often studied by recording electric potentials from the brain, either invasively or noninvasively, over repeated presentations of a sensory stimulus or task performance.[1] The traditional analysis framework models the recorded signal as the linear combination of background activity that is considered noise and evoked activity (signal) that is phase locked to event onset. This model, which we henceforth refer to as the signal-plus-noise (SPN) model, further assumes that the evoked response has a characteristic waveform whose amplitude and latency stay the same each time the event is repeated on multiple trials, and that the noise is not phase locked to the event and is uninformative. The signal is retrieved and noise eliminated by performing an average across an ensemble of trials triggered by the event onset. This simple averaging method has played a predominant role in cognitive neuroscience and contributed significantly to our understanding of brain functions. However, mounting evidence suggests that: (1) the background activity is not simply noise, but in fact contains high frequency oscillatory activity critical for cognitive performance[2] and (2) the amplitude and latency of the evoked signal is not invariant across trials, but vary significantly from trial to trial.[3–7] In this article we review some recent results where more realistic models of event-related

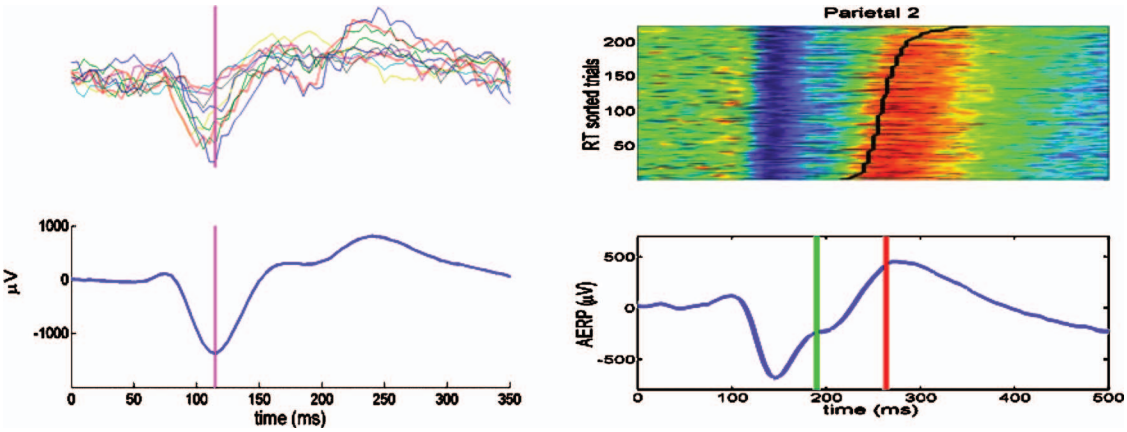

FIG. 1. (Color) Top left-hand panel: 50 single trial LFP time traces from a parietal channel. Lower left-hand panel: the average of 888 trials from the same channel and same experimental condition. Top right-hand: raster plot of 222 single-trial LFP time traces sorted according to the reaction time (RT) from a different parietal channel. Lower right-hand: average of the signals from the same channel. Time 0 denotes stimulus onset. Here AERP stands for average event-related potential.

signals are considered.[5–7] We start by presenting some evidence revealing the trial-to-trial variability in amplitude and latency of evoked responses and then propose a generative signal model, which we refer to as the variable-signal-plus-ongoing-activity (VSPOA) model, to describe both the variable evoked activity and ongoing activity. Based on the VSPOA model we describe a Bayesian analysis framework for separating evoked activity from ongoing activity. After such separation, the ongoing activity is treated as a piecewise stationary stochastic process and a multivariate autoregressive spectral analysis strategy is formulated to extract useful information including power, coherence, and Granger causality spectra from the ongoing activity. Some results of applications to neurobiological local field potential time series recordings are shown to demonstrate the utility of the VSPOA model and the effectiveness of the analysis strategy.

II. VARIABLE SIGNAL PLUS ONGOING ACTIVITY (VSPOA) MODEL

To motivate the VSPOA model we examine single-trial event-related time series and demonstrate the presence of the trial-to-trial variability in both amplitude and latency of stimulus evoked responses. In Fig. 1 (top left-hand side) we superimpose 50 single-trial local field potential (LFP) time traces recorded from the parietal cortex of a monkey performing a visuomotor task (see the following for experimental details).[8,9] The lower left-hand panel is the average using 888 trials from the same condition. The key observation is that much greater variability over trials is seen around the time of the N1 component, the peak time of which is indicated by the vertical bar, than during the time preceding the evoked activity (say 25 ms). The SPN model would predict the same degree of variability over trials at every point in the time series. Plotting ensemble variance as a function of time, careful analysis[5] attributes the increased ensemble variance around the N1 component to the trial-to-trial amplitude variability of the N1 component. In Fig. 1, the top right-hand panel is the raster plot of single-trial LFPs from another parietal electrode under the same condition sorted according to reaction time (RT). The LFP amplitude is coded by color. The ensemble average is shown in the lower right-hand panel. The latency of the evoked response clearly varies from one trial to the next. In addition, the latencies of different components vary with respect to one another, with the component around 280 ms clearly correlated with RT (the black curve).

The previous empirical evidence suggests that a generative model for the recorded single-trial LFP signal should incorporate at least four main properties in the event-related paradigm: (a) the existence of event-related signals that are relatively phase locked to a specific event onset; (b) the trial-to-trial variability in amplitude and latency of the event-related signals; (c) the possibility that the event-related response may be the superposition of multiple components with differential variability in their single-trial amplitudes and latencies; and (d) the existence of signals that are not phased locked to the event, including activity that is unrelated to the experiment (e.g., measurement noise) and activity that is induced by the event but not phase locked to it.[10] The model that incorporates these properties, which we call the VSPOA model, is written as[5–7]

$$x_r(t) = \sum_{n=1}^{N} a_{nr} s_n(t - \tau_{nr}) + \eta_r(t), \tag{1}$$

where $x_r(t)$ is the LFP recording from the rth trial, $s_n(t)$ is the nth event-related component waveform with trial-to-trial variable amplitude and latency given by a_{nr} and τ_{nr}, respectively, and N is the total number of components. The process $\eta_r(t)$, referred to as the ongoing activity, includes all the non-phase-locked signals and is assumed to have a zero mean.

The VSPOA model treats the recorded single-trial time series as composed of two distinct parts, evoked and ongoing activities. In Sec. III, we show that the parameters in the model, including the amplitude, latency, and the waveform of each evoked component, can be estimated in a Bayesian framework. After estimating the evoked signal on a single-trial basis, we obtain the ongoing activity as the residual of the recorded single-trial time series minus the evoked signal.

The ongoing activity is known to contain oscillatory activity that provides rich information about cognition.[2] Traditionally, the ongoing activity is extracted by removing the ensemble average from each trial. Careful analysis has shown that, in the face of trial-to-trial variability of stimulus evoked responses, this approach can lead to spurious results.[5] By modeling the event-related signal on a single-trial basis we can better recover the ongoing activity. In Sec. IV we describe an adaptive multivariate autoregressive modeling approach for analyzing the ongoing activity. The spectral quantities derived from this approach include power, coherence and Granger causality. Together they allow a detailed evaluation of synchronized neural activities in local as well as in large scale cortical networks.

III. SINGLE TRIAL ANALYSIS OF THE EVOKED ACTIVITY

Many current single-trial analysis methods are empirical and lack a rigorous theoretical foundation within which to understand the performance of the method and to refine the method in the face of complications inherent in real-world data. This realization has led us to the development of the following Bayesian approach which was first published in Ref. 6 from which the following text is adapted. A multivariate version of the approach has recently appeared in Ref. 7.

A. Bayesian estimation framework

The problem of estimating the single-trial parameters $s_n(t)$, a_{nr}, and τ_{nr} is formulated from a Bayesian perspective.[6] According to Bayes' theorem, the posterior probability of model parameters M given data D and prior information I, can be written as

$$p(M|D,I) = \frac{p(D|M,I)p(M|I)}{p(D|I)}. \tag{2}$$

For the VSPOA model in (1), the posterior probability becomes

$$p(\{s_n(t)\},\{a_{nr}\},\{\tau_{nr}\},\theta_\eta(t)|\{x_r(t)\},I)=\frac{p(\{x_r(t)\}|\{s_n(t)\},\{a_{nr}\},\{\tau_{nr}\},\theta_\eta(t),I)p(\{s_n(t)\},\{a_{nr}\},\{\tau_{nr}\},\theta_\eta(t)|I)}{p(\{x_r(t)\}|I)}, \tag{3}$$

where $\{\cdot\}$ refers to the set of parameters for all the components and the whole ensemble of trials, $\theta_\eta(t)$ denotes the parameters for the ongoing process and $p(\{s_n(t)\},\{a_{nr}\},\{\tau_{nr}\},\theta_\eta(t)|I)$ is the prior probability for the model parameters. For this additive model, the likelihood $p(\{x_r(t)\}|\{s_n(t)\},\{a_{nr}\},\{\tau_{nr}\},\theta_\eta(t),I)$ turns out to be simply given by the probability model of the ongoing activity, i.e., $p(\eta(t)|I)$. In the absence of precise knowledge about the temporal structure of the ongoing activity, we assign $\eta(t)$ to be independent identically distributed with a (unknown) time-independent variance σ_η^2 and zero mean. In this way, Eq. (3) is rewritten as

$$p(\{s_n(t)\},\{a_{nr}\},\{\tau_{nr}\},\sigma_\eta|\{x_r(t)\},I) = \frac{p(\{\eta(t)\}|\sigma_\eta,I)p(\{s_n(t)\},\{a_{nr}\},\{\tau_{nr}\},\sigma_\eta|I)}{p(\{x_r(t)\}|I)}. \tag{4}$$

Under the constraint of a given mean and σ_η^2 and following the principle of maximum entropy,[11] a Gaussian density is assigned to the likelihood function. After dropping the normalization term $1/p(\{x_r(t)\}|I)$, the posterior can be rewritten as

$$p(\{s_n(t)\},\{a_{nr}\},\{\tau_{nr}\},\sigma_\eta|\{x_r(t)\},I) \propto p(\{s_n(t)\},\{a_{nr}\},\{\tau_{nr}\},\sigma_\eta|I)(2\pi\sigma_\eta^2)^{-RT/2} \times\exp\left[\frac{-\Sigma_{r=1}^{R}\Sigma_{t=1}^{T}\left[x_r(t)-\Sigma_{n=1}^{N}a_{nr}s_n(t-\tau_{nr})\right]^2}{2\sigma_\eta^2}\right], \tag{5}$$

where R is the total number of trials and T is the total number of sampled data points in a given trial. For notational simplicity we have assumed the sampling interval to be unity in the previous expression. In practice, the real time can be recovered by multiplying the integer time index t by the sampling interval.

In the absence of detailed knowledge about the parameters a_{nr}, τ_{nr}, and $s_n(t)$, we take their prior distributions to be uniform, with appropriate cutoffs reflecting physiologically reasonable ranges of values. That is,

$$p(s_n(t)|I) = \text{const.}, \quad \forall\, n, \tag{6}$$

$$p(a_n|I) = \text{const.} \quad \text{for } 0 < a_n \le a_{\max}, \quad \forall\, n, \tag{7}$$

$$p(\tau_n|I) = \text{const.}, \quad \text{for } \tau_{\min} < \tau_n \le \tau_{\max}, \quad \forall\, n. \tag{8}$$

Treating the variance of the ongoing activity as a nuisance parameter and assigning the Jeffrey's prior $p(\sigma_\eta)=\sigma_\eta^{-1}$,[11] we marginalize the posterior over σ_η:

$$p(\{s_n(t)\},\{a_{nr}\},\{\tau_{nr}\}|\{x_r(t)\},I) \propto p(\{s_n(t)\},\{a_{nr}\},\{\tau_{nr}\}|I)\int_{-\infty}^{\infty}(2\pi\sigma_\eta^2)^{-RT/2}\sigma_\eta^{-1} \times\exp\left(-\frac{1}{2\sigma_\eta^2}\sum_{r=1}^{R}\sum_{t=1}^{T}\left[x_r(t)-\sum_{n=1}^{N}a_{nr}s_n(t-\tau_{nr})\right]^2\right)d\sigma_\eta, \tag{9}$$

and obtain

$$p(\{s_n(t)\},\{a_{nr}\},\{\tau_{nr}\}|\{x_r(t)\},I) \propto p(\{s_n(t)\},\{a_{nr}\},\{\tau_{nr}\}|I)(2\pi)^{-RT/2} \times\Gamma\left(\frac{RT}{2}\right)\left(\sum_{r=1}^{R}\sum_{t=1}^{T}\left[x_r(t)-\sum_{n=1}^{N}a_{nr}s_n(t-\tau_{nr})\right]^2\right)^{-RT/2}, \tag{10}$$

where $\Gamma(\cdot)$ is the gamma function.

The evaluation of the posterior probability and computation of its moments can be obtained via Markov chain Monte Carlo methods. Although highly informative, these methods carry the disadvantage of being computationally intensive. Here, instead, we summarize the posterior density by seeking the *maximum a posteriori* (MAP) solution, i.e., a set of parameters that maximize the posterior probability. In the context of (2), the MAP solution for the model parameters M is

$$\hat{M} = \arg\max_M[p(D|M,I)p(M|I)] = \arg\max_M[\ln p(M|I) + \ln p(D|M,I)]. \tag{11}$$

Because waveforms, amplitudes and latencies are being estimated simultaneously, the model has degeneracy. We solve this problem by constraining the ensemble mean of the amplitude and latency of each component to equal one and zero, respectively.

Intuition about the characteristics of the MAP solution can be gained by examining the partial derivatives of the logarithm of the posterior probability with respect to each of the model parameters. This leads to a practical and simple estimation algorithm. In what follows, the time t assumes discrete values corresponding to digital sampling. Let

$$Q = \sum_{r=1}^{R}\sum_{t=1}^{T}\left[x_r(t)-\sum_{n=1}^{N}a_{nr}s_n(t-\tau_{nr})\right]^2. \tag{12}$$

Let P represent the posterior probability in (11). Then its logarithm can be simply written as

$$\ln P = -\frac{RT}{2}\ln Q + \text{const}. \tag{13}$$

For the partial derivatives we use j,p,q to denote specific index values for the generic running indices n,r, and t, respectively. The first partial derivative with respect to $s_j(q)$ is

$$\frac{\partial \ln P}{\partial s_j(q)} = -\frac{RT}{2}Q^{-1}\frac{\partial Q}{\partial s_j(q)}, \tag{14}$$

where

$$\frac{\partial Q}{\partial s_j(q)} = -2\sum_{r=1}^{R}[Wa_{jr}-(a_{jr})^2 s_j(q)], \tag{15}$$

and

$$W = x_r(q+\tau_{jr}) - \sum_{n=1,n\neq j}^{N}a_{nr}s_n(q-\tau_{nr}+\tau_{jr}). \tag{16}$$

Setting $\partial Q/\partial s_j(q)=0$ gives

$$\hat{s}_j(q) = \frac{\sum_{r=1}^{R}Wa_{jr}}{\sum_{r=1}^{R}(a_{jr})^2}, \tag{17}$$

with $\hat{s}_j(q)$ denoting the estimated parameter. The previous equation does not have a closed-form solution as the right-hand side depends on the other estimated parameters. However, intuition about the type of solution can be obtained by examining the term W. Basically, this term involves the following two elements: (a) the data is shifted according to the latency of the estimated component, i.e., $x_r(q+\tau_{jr})$ and (b) the other scaled and time shifted components, i.e., $a_{nr}s_n(q-\tau_{nr}+\tau_{jr})$, for $n\neq j$ are subtracted from the data. The properly scaled residuals, where the scaling is given by the term a_{jr}, are then averaged across trials.

Similarly, we obtain the estimate for the amplitude a_{nr}:

$$\hat{a}_{jp} = \frac{\sum_{t=1}^{T}UV}{\sum_{t=1}^{T}V^2}, \tag{18}$$

where $U=x_p(t)-\sum_{n=1,n\neq j}^{N}a_{np}s_n(t-\tau_{np})$ and $V=s_j(t-\tau_{jp})$. Notice that the formula derived for $\hat{a}_{jp}$ is related to a matched filter solution. That is, $\hat{a}_{jp}$ is given by projecting U, which is the data after removing the contribution from the other scaled and time shifted components, onto V, which is the current component under estimation.

For the latency estimation, setting $\partial Q/\partial\tau_{jp}=0$ leads to the following equation:

$$2\sum_{t=1}^{T}\left[\left[x_p(t)-\sum_{\substack{n=1\\n\neq j}}^{N}a_{np}s_n(t-\tau_{np})\right]a_{jp}s_j'(t-\tau_{jp}) - a_{jp}^2 s_j'(t-\tau_{jp})s_j(t-\tau_{jp})\right]=0, \tag{19}$$

where $s_j'(t-\tau_{jp})$ is the time derivative of $s_j(t-\tau_{jp})$. The solution for $\hat{\tau}_{jp}$ is more difficult as τ appears in the argument of the waveform function. Again, intuition can be gained by directly examining the condition for the maximization of the logarithm of the posterior, which is equivalent to the minimization of the term Q in (12). Expansion of this term results in

$$\sum_{r=1}^{R}\sum_{t=1}^{T}\left[x_r^2(t)+\left[\sum_{n=1}^{N}a_{nr}s_n(t-\tau_{nr})\right]^2 - 2x_r(t)\sum_{n=1}^{N}a_{nr}s_n(t-\tau_{nr})\right]. \tag{20}$$

As τ_{jp} is varied, only the cross terms in $x_p(t)\Sigma_{n=1}^{N}a_{np}s_n(t-\tau_{np})$, for $n=j$ are relevant for the minimization of (12) (as long as the event-related components $s_n(t)$ can be considered zero outside some time interval (t_0,t_f)). Thus the optimal parameter $\hat{\tau}_{jp}$ is found by maximizing

$$\rho(\tau) = \sum_{t=1}^{T}\left[a_{jp}s_j(t-\tau)\left[x_p(t)-\sum_{n=1,n\neq j}^{N}a_{np}s_n(t-\tau)\right]\right], \tag{21}$$

which, if properly normalized, is just the cross correlation between the estimated component and the data after the con-

tributions from the other components have been subtracted out. Thus,

$$\hat{\tau}_{jp} = \arg\max_{\tau} \rho(\tau). \tag{22}$$

This result corresponds to Woody's matched filter algorithm for latency estimation.[3]

B. Algorithm implementation

The analysis in the previous section suggests a simple heuristic algorithm. After an initial guess, at each iteration step, the parameters for all components are updated in sequence as mentioned before: first the latency, then the waveforms, and finally the amplitude. Specifically, let $s_j^m(t)$, a_{jr}^m, τ_{jr}^m denote the estimated values of the parameters in the mth iteration. Also, let the latency assume only discrete integer values, with units corresponding to the sampling interval. To avoid degeneracy in the model, the averages of the amplitudes and latencies in each iteration are constrained to $\langle a_{jr}^m \rangle_r \equiv 1$ and $\langle \tau_{jr}^m \rangle_r \equiv 0$. In this way, if there is no trial-to-trial variability both in amplitude and latency, the superposition of the estimated component waveforms should equal the simple average. For a single channel data set $\{x_r(t)\}$, the algorithm consists of the following steps:

(1) At $m=0$, the initial guess for the amplitudes and latencies are set to $a_{jr}^0=1$, $\tau_{jr}^0=0$, $\forall j,r$. For simplicity, the decision on the number of components N is based on inspection of the average event-related potential (AERP) according to conventionally defined ERP components.[10] (A more statistically principled way of determining N can be found in Ref. 7.) Similarly, N nonoverlapping segments of the AERP are taken as the initial guesses for the N components' waveforms $s_j^0(t)$. After this initialization, each iteration consists of four steps:

(2) For all the trials, estimate the single-trial latencies for one component at a time, starting with the first and proceeding up to the Nth component, according to $\tau_{jr}^{m+1} = \arg\max_\tau \rho^m(\tau)$. Re-expressed in time units, the estimated latency is simply $\tau_{jr}\Delta t$, where Δt is the sampling interval. Given an approximate knowledge of where in time the component is expected to happen, an interval for the search of the optimal latency τ_{jr} can be stipulated. In this way, the possibility that the component matches by chance the waveform of unrelated ongoing activity is diminished.

(3) Estimate the waveforms according to

$$s_j^{m+1}(t) = \frac{\sum_{r=1}^R W a_{jr}^m}{\sum_{r=1}^R (a_{jr}^m)^2},$$

with

$$W = x_r(t + \tau_{jr}^{m+1}) - \sum_{n=1, n\neq j}^{N} a_{nr}^m s_n^m (t - \tau_{nr}^{m+1} + \tau_{jr}^{m+1}).$$

(4) For all the trials and components, estimate the amplitude according to:

$$a_{jr}^{m+1} = \frac{\sum_{t=1}^T UV}{\sum_{t=1}^T V^2},$$

with $U = x_r(t) - \sum_{n=1,n\neq j}^N a_{nr}^m s_n^{m+1}(t - \tau_{nr}^{m+1})$ and $V = s_j^{m+1}(t - \tau_{jr}^{m+1})$.

(5) Increment the iteration index: $m=m+1$; repeat steps (1)–(4) for M iterations.

We note that the differential variability of the components on a trial-by-trial basis is the foundation of the estimation technique. We thus term our algorithm differentially variable component analysis (dVCA).[6,7]

C. Application to local field potential recordings

The experimental data used in this study was collected by Dr. Richard Nakamura in the Laboratory of Neuropsychology at the U. S. National Institute of Mental Health.[8,9] We henceforth refer to the dataset as the Nakamura data set. In this experiment, differential LFPs were simultaneously recorded from surface-to-depth bipolar Teflon-coated platinum electrodes, chronically implanted at up to 16 sites distributed over either the left-hand or the right-hand cerebral hemisphere, contralateral to the preferred hand, of four highly trained macaque monkeys performing a visuomotor pattern discrimination task. (Here differential bipolar recordings are essential for generating local signals by rejecting common mode and volume conduction.) The sampling rate was 200 Hz. The monkey initiated each trial by depressing and holding steady a mechanical lever with the preferred hand and began to anticipate the imminent onset of visuomotor processing. The anticipation period lasted 1 s on average. Data collection commenced about 115 ms prior to stimulus onset (time 0) and continued until 500 ms poststimulus. Each stimulus consisted of four dots arranged as a (left- or right-hand slanted) line or diamond on a display screen. The monkey indicated whether the stimulus was a line or diamond pattern by a GO (lever release) or NOGO (pressure maintenance) response. GO and NOGO trials were presented with equal probability in around 1000-trial sessions. The response contingency was randomly switched across sessions.

Consider the case in the top right-hand panel of Fig. 1 in which 222 GO response single-trial time series from a parietal channel are displayed as a raster plot. Here diamond is the stimulus. Two components were identified and their estimated waveforms are shown in Fig. 2 (top panel). Single-trial amplitude and latency distributions for both components are displayed in Fig. 2, middle and bottom panels, respectively. The two latency histograms both exhibit a single peak distribution, suggesting that the estimation captured the latencies of the underlying single-trial events that were relatively phase locked to the stimulus onset.

By inspecting the raster plot in Fig. 1 it is apparent that, the latency of the second component (200–320 ms) clearly tracks the RT and should have a positive correlation with RT on a trial-by-trial basis, whereas the first component does not have such a clear tendency. We tested this intuitive observation. Figure 3 replicates the average evoked response shown in the bottom right-hand panel of Fig. 1, with vertical lines now demarcating the time regions of the main peaks of the two estimated components (top panel). Scatter plots of the latency estimates for each component with RT are shown in the bottom panel of Fig. 3. The r^2 values were found to be 0.09 and 0.25 for the first and second components, the r^2 value for the second component being significantly greater

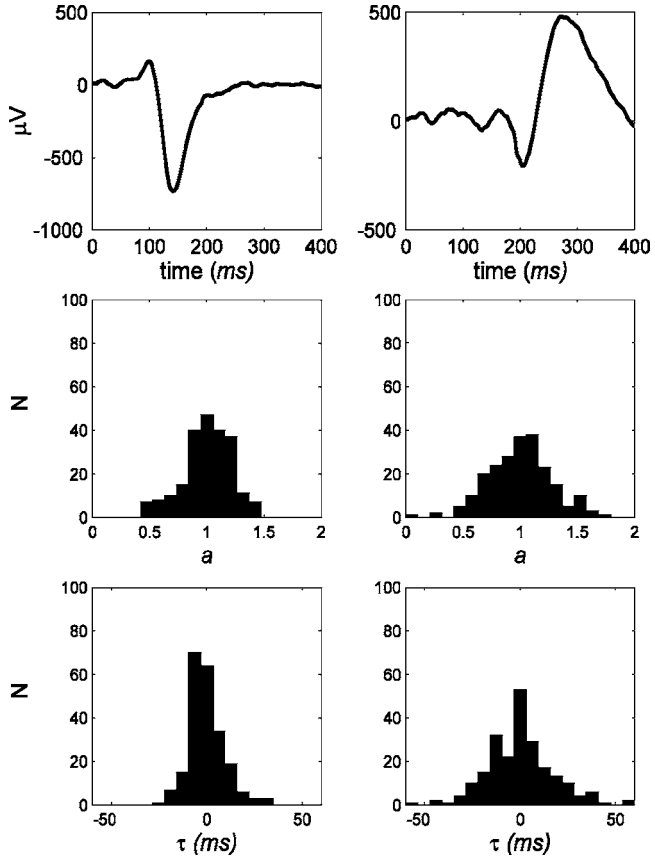

FIG. 2. Top: two estimated component waveforms; middle: amplitude distributions of the two components; and bottom: latency distribution of the two components. Taken from Ref. 6.

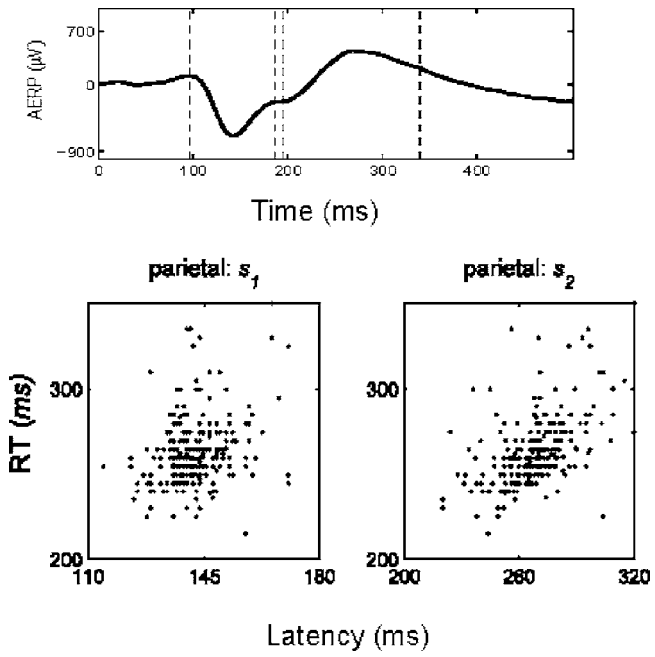

FIG. 3. Average evoked response for the parietal channel in Fig. 1(top right-hand panel). Latency vs RT for the two components. Taken from Ref. 6.

than that of the first ($p<0.02$), confirming the closer relation of the second component to RT as was observed in the raster plot from Fig. 1.

IV. SPECTRAL ANALYSIS OF THE ONGOING ACTIVITY

It is known that ongoing neural activity plays an important role in the cognitive operations of the brain.[2,12] As ongoing activity is usually embedded in event-related activity, more accurate signal models, such as the VSPOA model proposed here, help to better estimate ongoing activity. Using the VSPOA model in step (1), we write the ongoing activity, $\hat{\eta}_r(t)$, so estimated, as

$$\hat{\eta}_r(t) = x_r(t) - \sum_{n=1}^{N} \hat{a}_{nr}\hat{s}_n(t-\hat{\tau}_{nr}), \tag{23}$$

which is performed on each trial for every recording channel.

When multiple, spatially distributed channels are recorded, examination of the interactions between channels is of general interest. In the following, we present a short-window adaptive multivariate autoregressive (AMVAR) method to perform spectra analysis on the ongoing activity.[13]

A. Short window AMVAR spectral analysis

Let p channels of ongoing activity at time t be denoted by $\boldsymbol{\eta}_t=(\eta_{1t},\eta_{2t},\ldots,\eta_{pt})^T$ where T stands for matrix transposition. Assume that the data over an analysis window are described by a multivariate autoregressive (MVAR) model:

$$\sum_{k=0}^{m} \mathbf{A}_k \boldsymbol{\eta}_{t-k} = \mathbf{E}_t, \tag{24}$$

where $\mathbf{E}_t$ is a temporally uncorrelated residual error series with covariance matrix $\boldsymbol{\Sigma}$, and $\mathbf{A}_k$ are $p\times p$ coefficient matrices which are obtained by solving the multivariate Yule-Walker equations (of size mp^2) using the Levinson, Wiggins, and Robinson algorithm.[13] Here repeated trials for the same experimental condition are treated as realizations of a piecewise stationary stochastic process. The order m of the MVAR model was determined by the Akaike information criterion (AIC),[14] a quantity based on the tradeoff between sufficient spectral resolution and overparameterization. Once the model coefficients $\mathbf{A}_k$ and $\boldsymbol{\Sigma}$ are estimated, the spectral matrix can be evaluated as

$$\mathbf{S}(f) = \langle \boldsymbol{\eta}(f)\,\boldsymbol{\eta}^*(f)\rangle = \mathbf{H}(f)\boldsymbol{\Sigma}\mathbf{H}^*(f), \tag{25}$$

where the asterisk denotes matrix transposition and complex conjugation, $\langle . \rangle$ stands for the ensemble average, and $\mathbf{H}(f)=(\Sigma_{k=0}^{m}\mathbf{A}_k e^{-2\pi ikf})^{-1}$ is the transfer function of the MVAR model. The power spectrum of channel l is given by $S_{ll}(f)$ which is the lth diagonal element of the spectral matrix $\mathbf{S}(f)$. The coherence spectrum between channel l and channel k is

$$C_{lk}(f) = |S_{lk}(f)|/(S_{ll}(f)S_{kk}(f))^{1/2}. \tag{26}$$

The value of coherence can range from 1, indicating maximum linear interdependence between channel l and channel k at frequency f, down to 0, indicating no linear interdepen-

dence. The phase of the complex quantity $S_{lk}(f)$ plotted as a function of f gives the phase spectrum.

Granger causality is a quantity for assessing the directional interdependence between channels. When a bivariate autoregressive model is estimated for a given channel pair, k and l, according to the procedure described earlier, Granger causality spectral estimates can be computed according to Geweke's formulation as[15–17]

$$I_{k\to l}(f) = -\ln\left(1 - \frac{\left(\Sigma_{kk} - \Sigma_{lk}^2/\Sigma_{ll}\right)|H_{lk}(f)|^2}{S_{ll}(f)}\right) \tag{27}$$

and

$$I_{l\to k}(f) = -\ln\left(1 - \frac{\left(\Sigma_{ll} - \Sigma_{kl}^2/\Sigma_{kk}\right)|H_{kl}(f)|^2}{S_{kk}(f)}\right), \tag{28}$$

where Σ_{kk}, Σ_{ll}, Σ_{kl}, and Σ_{lk} are elements of the covariance matrix for the noises in the bivariate autoregressive model on channels k and l, and S_{kk} and S_{ll} are the power spectra of channel k and l, respectively.

In a typical cognitive experiment the brain undergoes rapid transitions in its functional state, from anticipation to sensation to decision making to movement execution, all within 300-400 ms. This implies that the ongoing activity recorded during a trial may be nonstationary. The strategy we adopt here is to assume that the data can be treated as piecewise stationary in intervals on the order of 50-100 ms. Computation of the MVAR model in a short analysis window, which adapts to the temporally localized within-window dynamics as it is shifted along the entire trial, constitutes the AMVAR approach, yielding a finely resolved temporal picture of cortical cognitive dynamics.

B. Model validation, variability assessment and significance testing

According to the methodology outlined previously, spectral quantities such as power, coherence and Granger causality are estimated once a MVAR model has been fitted to the data within a given short analysis window from many trials. It is thus critical that the MVAR model properly represents the statistical properties of the time series data. A number of model validation steps were designed to ensure this. (a) A model order is suitably identified by the AIC criterion.[14] The statistical results should be robust against small variations in the model order. (b) For the MVAR model to adequately represent the data set, the residual error process should be uncorrelated (white noise). A white noise residual is a strong indication that the data are well represented by the MVAR model.[18] Thus, one examines whether the whiteness requirement is met after the model has been fit.[13] (c) As a cross-validation step we also compute spectral quantities from the same data using other methods.[19] We only proceed with the AMVAR methodology after obtaining similar results with these other methods.

To assess the variability of the spectral quantities derived from the MVAR model, we use a bootstrap resampling technique.[20] It involves randomly sampling a pool of trials with replacement from the total ensemble, and then estimating the MVAR model for this pool. Repeating this process many times for different pools of the same size we estimate the mean and standard deviation of any given spectral quantity over the whole collection of estimated bootstrap values. The standard deviation gives a measure of the variability of the estimator.[13]

For interdependence measures such as coherence and Granger causality, we have adopted a random permutation technique[16,17] to build a baseline for statistical significance assessment which is similar to the shift-predictor approach used in other applications.[21] Consider two channels of recordings with many repeated trials. We can reasonably assume that the data from different trials are independent of one another. Randomly pairing data for channel 1 with data for channel 2 from a different trial leads to the creation of a synthetic ensemble of trials. In this synthetic ensemble, no interdependence between the two channels is expected, due to the construction, yet the temporal structure within a channel is preserved. Performing such random pairing with many different permutations produces a distribution of coherence or causality spectra corresponding to the null hypothesis (i.e., a distribution under the condition of no statistical interdependence). Then the distribution for a given statistic from bootstrapping the actual data is compared with this baseline null hypothesis distribution for the assessment of significance levels.

C. Application to local field potential recordings

The same Nakamura dataset as that used in Sec. III is considered here. MVAR spectral analysis is applied to the ongoing activity. Past work has identified a set of channels in sensorimotor cortex forming a synchronized beta oscillatory network related to the facilitation of motor maintenance in the period before stimulus presentation.[16] Figure 4 shows the average power, coherence and Granger causality spectra for

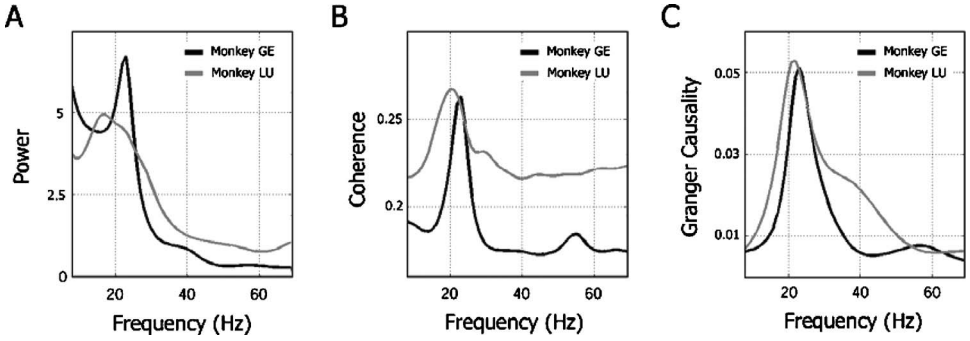

FIG. 4. (A) Mean power spectra averaged over all recording sites, (B) mean coherence, and (C) mean Granger causality spectra averaged over all significant site pairs. Taken from Ref. 16.

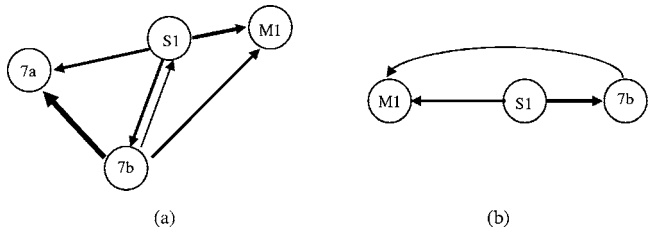

FIG. 5. Granger causality graphs for the beta oscillatory network in sensorimotor cortex of (a) the right-hand hemisphere of GE and (b) the left-hand hemisphere of LU. Adapted from Ref. 22.

two subjects (GE and LU). Consistent peaks around 20 Hz are seen in all spectral quantities, indicating that synchronized beta-range oscillations are present in local neuronal assemblies at the recording sites, and that the oscillations bind together the local assemblies into a large-scale sensorimotor network.

To further understand the functional role of each cortical site we plot Granger causality graphs in Fig. 5.[22] The thickness of the lines connecting recording sites encodes the magnitude of significant causality values at the peak frequency. Three cortical areas are common to the graphs of both monkeys: primary motor (M1), primary somatosensory (S1), and posterior parietal area 7b. Among the sites in these three areas, Granger causal influence patterns common to both monkeys are: (1) S1$\rightarrow$M1, (2) S1$\rightarrow$7b, and (3) 7b$\rightarrow$M1. There is an additional small influence from 7b to S1 in the graph of one monkey. These patterns suggest the hypothesis that the beta oscillation network exists to support the maintenance of steady pressure on the depressed lever. The reasons are as follows. First, steady pressure maintenance is akin to closed loop control, and as such, sensory feedback is expected to provide the input needed for cortical assessment of the current state of behavior. It is well known that the maintenance of sustained motor output is severely impaired when somatosensory input is lacking.[23] This notion is consistent with our observation that primary somatosensory area S1 serves as the dominant source of causal influences to other areas in the network. Second, posterior parietal area 7b is known to be involved in the control of nonvisually guided movement and, as a higher-order association area, it may maintain representations relating to the current goals of the motor system.[24] This would imply that area 7b receives sensory updates from area S1 and outputs correctional signals to the motor cortex (M1). This conceptualization is consistent with the causality patterns in Fig. 5. Third, previous work has implicated beta-range oscillations as a neural correlate of isometric pressure maintenance in the motor cortex.[25,26] Our work demonstrates that a sensorimotor beta network exists on a much larger scale, with postcentral areas (i.e., S1 and 7b) playing a key role in organizing the network dynamics. We emphasize that the latter conclusion is made possible by the directional information provided by Granger causality.

V. SUMMARY

Recognizing the trial-to-trial variability of event-related responses and the importance of ongoing activity, we propose a VSPOA model to capture the statistical characteristic of neurobiological time series obtained from typical cognitive experiments. An algorithm based on Bayesian inference, called differentially variable component analysis (dVCA), is shown to provide reliable estimates of the single-trial parameters in the model. Ongoing activity is better estimated by employing the more realistic VSPOA model than the simple SPN model. An MVAR modeling approach is adopted to describe the temporal dynamics of ongoing activity. From each MVAR model we derive power, coherence and Granger causality spectra. These quantities provide the basis for understanding the role of ongoing activity in cognition and motor control. Applications to neurobiological local field potential time series recordings are used to illustrate the effectiveness of the approach.

ACKNOWLEDGMENTS

The work was supported by NIH Grant Nos. MH071620, MH070498, MH064204, and NS054314.

[1] S. L. Bressler and M. Ding, in *Encyclopedia of Biomedical Engineering*, edited by M. Akay (Wiley, New York, in press).
[2] H. Liang, S. L. Bressler, M. Ding, W. A. Truccolo, and R. Nakamura, NeuroReport **13**, 2011–2015 (2002).
[3] C. D. Woody, Med. Biol. Eng. **5**, 539–553 (1967).
[4] R. Coppola, R. Tabor, and M. S. Buchsbaum, Electroencephalogr. Clin. Neurophysiol. **44**, 214–222 (1978).
[5] W. A. Truccolo, M. Ding, K. H. Knuth, R. Nakamura, and S. L. Bressler, Clin. Neurophysiol. **113**, 206–226 (2002).
[6] W. Truccolo, K. H. Knuth, A. Shah, S. L. Bressler, C. E. Schreoder, and M. Ding, Biol. Cybern. **89**, 426–438 (2003).
[7] K. H. Knuth, A. S. Shah, W. A. Truccolo, M. Ding, S. L. Bressler, and C. E. Schroeder, J. Neurophysiol. **95**, 3257–3276 (2006).
[8] S. L. Bressler, R. Coppola, and R. Nakamura, Nature (London) **366**, 153–156 (1993).
[9] A. Ledberg, S. L. Bressler, M. Ding, R. Coppola, and R. Nakamura, Cereb. Cortex (in press).
[10] G. R. Mangun, in *Induced Rhythms in the Brain*, edited by E. Basar and T. H. Bullock (Birkhauser, Boston, 1992), pp. 217–231.
[11] D. S. Sivia, *Data Analysis: A Bayesian Tutorial* (Oxford Clarendon, New York, 1996).
[12] A. Arieli, A. Sterkin, A. Grinvald, and A. Aertsen, Science **273**, 1868–1871 (1996).
[13] M. Ding, S. L. Bressler, W. Yang, and H. Liang, Biol. Cybern. **83**, 35–45 (2000).
[14] H. Akaike, IEEE Trans. Autom. Control **19**, 716–723 (1974).
[15] J. Geweke, J. Am. Stat. Assoc. **77**, 304–313 (1982).
[16] A. Brovelli, M. Ding, A. Ledberg, Y. Chen, R. Nakamura, and S. L. Bressler, Proc. Natl. Acad. Sci. U.S.A. **101**, 9849–9854 (2004).
[17] M. Ding, Y. Chen, and S. L. Bressler, in *Handbook of Time Series Analysis*, edited by J. Timmer, B. Schelter, and M. Winderhalder (Wiley-VCH, Berlin, in press).
[18] H. Lutkepohl, *Introduction to Multiple Time Series Analysis* (Springer, New York, 1993).
[19] P. P. Mitra and B. Pesaran, Biophys. J. **76**, 691–708 (1999).
[20] B. Efron, *The Jackknife, the Bootstrap, and Other Resampling Plans* (SIAM, Philadelphia, 1982).
[21] N. G. Hatsopoulos, C. L. Ojakangas, L. Paninski, and J. P. Donoghue, Proc. Natl. Acad. Sci. U.S.A. **95**, 15706–15711 (1998).
[22] Y. Chen, S. L. Bressler, and M. Ding, J. Neurosci. Methods **150**, 228–237 (2006).
[23] J. C. Rothwell, M. M. Traub, B. L. Day, J. A. Obeso, P. K. Thomas, and C. D. Marsden, Brain **105**, 515–542 (1982).
[24] M. F. S. Rushworth, P. D. Nixon, and R. E. Passingham, Exp. Brain Res. **117**, 292–310 (1997).
[25] J. N. Sanes and J. P. Donoghue, Proc. Natl. Acad. Sci. U.S.A. **90**, 4470–4474 (1993).
[26] S. N. Baker, E. Olivier, and R. N. Lemon, J. Physiol. (London) **501**, 225–241 (1997).